

Engineering Metamaterial Interface Scattering Coefficients via Quantum Graph Theory

T.M. LAWRIE^a, G. TANNER^{a,*} AND G.J. CHAPLAIN^b

^a*School of Mathematical Sciences, University of Nottingham, NG7 2RD, United Kingdom*

^b*Centre for Metamaterial Research and Innovation, Department of Physics and Astronomy, University of Exeter, Exeter EX4 4QL, United Kingdom*

Doi: [10.12693/APhysPolA.144.486](https://doi.org/10.12693/APhysPolA.144.486)

*e-mail: gregor.tanner@nottingham.ac.uk

For layered metamaterial devices, the reflection and transmission coefficients at an interface typically depend on the properties of the coupling between different layers. In this paper, we set out to engineer the reflection/transmission behaviour at boundaries to obtain desirable properties such as achieving total reflection and transmission. Based on the quantum graph formulation for modelling metamaterials developed in *Sci. Rep.* **12**(1), 18006 (2022), we tailor the interface reflection and transmission coefficients by patterning the boundary with resonant elements at each interface vertex. By tuning the internal lengths of the resonant elements, we demonstrate both minimization and maximization of the reflection coefficient via a scattering formulation. In addition, we present an interface set-up incorporating beyond-nearest-neighbour connections, which yields narrow-band transmission for certain angles only, creating an angular filtering interface.

topics: quantum graph theory, wave scattering, metamaterials, wave propagation

1. Introduction

Over recent decades, the field of metamaterial research has grown rapidly with the intent of engineering materials with special electromagnetic and acoustic wave properties, see for example [1] for an overview. Typically, metamaterial properties are given by a unit cell resonant or phase modulating characteristics. Recently, also non-local or beyond-nearest-neighbour interactions [2] have been investigated. These structures have additional coupling terms due to connections that extend beyond the periodic unit cell; numerical and experimental realisations have been studied both in an acoustics and elasticity setting [3–6]. Customisation procedures have been developed to engineer the dispersion behaviour of metamaterials using competing channels of the power flowing through the structure [7]. In numerical simulations, the governing models have, so far, been based on analogies to systems of coupled masses and springs akin to the canonical model used by Brillouin [8]. In this paper, we model metamaterials via quantum graph theory instead, first introduced by Lawrie et al. [9]. The wave dynamics takes place here along one-dimensional edges coupled at vertices on an infinite periodic graph network. Resonant characteristics can be introduced in the form of vertex scattering conditions. The model provides a fast and flexible tool for designing metamaterials and for uncovering new and interesting wave phenomena.

Quantum graph theory was initially formulated by Kottos and Smilansky [10] in order to study the quantum mechanical properties of complex systems; for a comprehensive introduction, see [11, 12]. The simple mathematical construction of quantum graphs naturally leads to a great number of interdisciplinary applications, such as the study of quantum chaos [11], modelling the vibrations of coupled plates [13], formulating quantum random walks [14, 15] and quantum search algorithms [16]. The graph formalism allows the eigenvalue conditions to be written in terms of a secular equation for a matrix of finite dimension. Similarly, the scattering matrix of an open quantum graph can be given as a closed-form expression involving finite dimensional matrices. Closed-form expressions of the Green's function of a quantum graph have been given in [17]. Infinite periodic quantum graphs allow for a spectral analysis where an underlying graph “decoration” can be chosen to create spectral gaps [18]. For such infinite periodic graph structures, it has furthermore been shown by Exner et al. [19] that the spectrum of the graph Hamiltonian converges to the corresponding Schrödinger operator on the Euclidean space in the continuum limit. This makes the mathematical language of quantum graph theory an ideal tool for modelling metamaterial set-ups using a continuum limit formulation.

Describing wave coupling between different media is a key problem in metamaterial research and the motivation for this work. The ability to efficiently

model such an interface permits an additional degree of freedom for metamaterial design, which has recently received attention in the context of homogenisation [20]. At a metamaterial interface, the boundary reflection coefficients depend strongly on the properties of the interface layer connecting the two metamaterials. In order to tune the reflection behaviour, we use and expand on tools introduced in [9]. We tailor the interface scattering coefficients by decorating the boundary with resonant elements at each interface vertex. By varying the underlying graph structure, we demonstrate the tunability of the reflection/transmission behaviour ranging from total reflection to total transmission. This formulation is then used to construct a beam splitting and steering device with minimal reflection — a primitive cloak. In addition, we present scattering effects when introducing a beyond-nearest-neighbour structure at the boundary. We find rapid switching between full reflection and transmission as a function of the angle of incident, that is, the interface acts as an angular filtering device.

The paper is structured as follows: In Sect. 2, we introduce the general quantum graph formalism for modelling metamaterials based on the theory developed in [9]. In Sect. 2.1, the wave dynamics on the graph is defined, and in Sect. 2.2, it is shown how the compact portions of the graph at each vertex are reduced to simple frequency-dependent point scatterers. The eigenfunction solutions on the periodic quantum graph are introduced in Sect. 2.3 and combined to form Gaussian beam solutions in Sect. 2.4. In Sect. 3, we derive the scattering matrix for a boundary layer or interface connecting two metamaterials. We demonstrated the efficiency and flexibility of the quantum graph approach by showing various example set-ups in Sect. 3.2. In particular, modifications for obtaining resonant interfaces giving zero and full reflection, as well as a configuration displaying both beam splitting and reconfiguration, are shown in Sect. 3.2.1. Finally, in Sect. 3.2.2, the effects of introducing a beyond-nearest-neighbour interface are formulated, showing interesting angle filtering properties.

2. Metamaterials: The quantum graph formalism

2.1. General set-up

We will provide a brief introduction to the quantum graph model for metamaterials here; for more details, see [9]. Typically, metamaterials are constructed from a periodic arrangement of sub-wavelength resonant elements. We consider each such element as an open quantum graph $\Gamma(\mathcal{V}, \mathcal{E}, L)$, where \mathcal{V} is a finite set of vertices with imposed boundary conditions connected by a finite set of bidirectional edges \mathcal{E} with metric length $L = \{\ell_j : j \in \mathcal{E}\}$. Edges of finite length will be called bonds

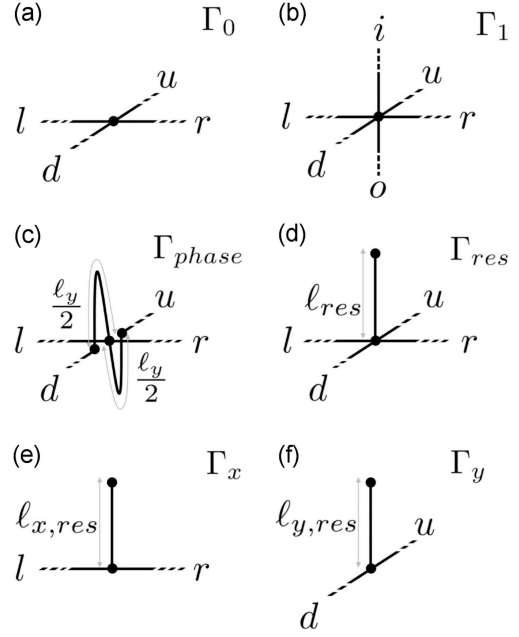


Fig. 1. Six examples of sub-wavelength resonant or phase modulating elements are shown labelled here as Γ_x , Γ_y , Γ_0 , Γ_1 , Γ_{res} , and Γ_{phase} . The bond lengths are shown as $\ell_{x,res}$, $\ell_{y,res}$, ℓ_{res} , and ℓ_y . In turn, the lead directions are given by l , r , d , u , i , and o . The graph in (c) represents a phase modulator, the graph in (d) represents a resonator on a vertex, and (e) and (f) resonant resonators on an edge.

\mathcal{B} with coordinate $z_j = [0, \ell_j]$ with reverted edge coordinate given by $\tilde{z}_j = \ell_j - z_j$. Edges of infinite length will be called leads \mathcal{L} with coordinate $z_j = [0, \infty)$ and no reverted edge coordinate. Naturally, $\mathcal{E} = \mathcal{B} \cup \mathcal{L}$. The resonant characteristics of an element are determined by treating the compact portion of the graph as a scattering site, as shown in Fig. 1. The construction of the corresponding scattering matrix is described in Sect. 2.2. The open graphs are then arranged and connected to form a mesh with square periodic topology embedded in \mathbb{R}^2 and discussed in more detail in Sect. 2.3. For this construction, four leads $\mathcal{L} = \mathcal{L}_l, \mathcal{L}_r, \mathcal{L}_d, \mathcal{L}_u$ are imposed on the compact portion of the graph in the left (l), right (r), down (d), and up (u) directions. In the example in Fig. 1b, two additional leads, \mathcal{L}_i and \mathcal{L}_o , have been added, heading in (i) and out (o) of the plane and allowing for beyond-nearest-neighbour connections discussed in more detail in Sect. 3.1. All edges in \mathcal{E} are endowed with the Helmholtz wave equation with wave number k , i.e.,

$$\left(\frac{\partial^2}{\partial z_j^2} + k^2 \right) \psi_j(z_j) = 0. \quad (1)$$

The solutions are given as a superposition of counter-propagating plane waves on a given edge $j \in \mathcal{E}$, i.e.,

$$\psi_j(z_j) = e^{ikz_j} a_j^{\text{out}} + e^{-ikz_j} a_j^{\text{in}}. \quad (2)$$

Here, $a_j^{\text{out/in}}$ represents the complex wave amplitudes heading out of or into a vertex. The edge solutions can then be concatenated to form the vector $\Psi(\hat{Z}) = (\Psi_{\mathcal{L}}(\hat{Z}), \Psi_{\mathcal{B}}(\hat{Z}))^T$ of all lead and bond solutions, where

$$\Psi(\hat{Z}) = e^{ik\hat{Z}} \mathbf{a}^{\text{out}} + e^{-ik\hat{Z}} \mathbf{a}^{\text{in}}. \quad (3)$$

Here, $\mathbf{a}^{\text{out/in}} = (\mathbf{a}_{\mathcal{L}}^{\text{out/in}}, \mathbf{a}_{\mathcal{B}}^{\text{out/in}})^T$ represents the vector of all complex wave amplitudes, and \hat{Z} is a diagonal matrix of all edge coordinates. Given the general solutions, we can treat the compact portion of the graph as a scattering site and thus derive a resonant element scattering matrix \hat{S}_Γ .

2.2. The unit cell scattering matrix

Wave transport along each bond can be modelled by mapping the outgoing wave amplitudes at vertices to the incoming wave amplitudes at adjacent vertices by a matrix $\hat{P}(k; L)$,

$$\mathbf{a}_{\mathcal{B}}^{\text{in}} = \hat{P}(k; L) \mathbf{a}_{\mathcal{B}}^{\text{out}}. \quad (4)$$

The matrix elements of \hat{P} take account of the phase $e^{ik\ell_j}$ accumulated by the wave as it travels along a given bond j . The wave amplitudes on different edges are mapped from incoming to outgoing wave amplitudes at the vertices via a vertex scattering matrix $\hat{\sigma}$ that satisfies the imposed vertex boundary conditions, i.e.,

$$\begin{aligned} \mathbf{a}^{\text{out}} &= \hat{\sigma} \mathbf{a}^{\text{in}}, & \text{or in block form} \\ \begin{pmatrix} \mathbf{a}_{\mathcal{L}}^{\text{out}} \\ \mathbf{a}_{\mathcal{B}}^{\text{out}} \end{pmatrix} &= \begin{pmatrix} \hat{\sigma}_{\mathcal{L}\mathcal{L}} & \hat{\sigma}_{\mathcal{L}\mathcal{B}} \\ \hat{\sigma}_{\mathcal{B}\mathcal{L}} & \hat{\sigma}_{\mathcal{B}\mathcal{B}} \end{pmatrix} \begin{pmatrix} \mathbf{a}_{\mathcal{L}}^{\text{in}} \\ \mathbf{a}_{\mathcal{B}}^{\text{in}} \end{pmatrix}. \end{aligned} \quad (5)$$

For this work, we assume Neumann–Kirchhoff boundary conditions [11] at each vertex, giving the pq -th matrix element of $\hat{\sigma}$ associated with vertex V_j as

$$[\hat{\sigma}_{V_j}]_{pq} = \frac{2}{v_{V_j}} - \delta_{pq}. \quad (6)$$

Note that the index j runs now over the number of vertices \mathcal{V} in Γ . Here, δ_{pq} is the Kronecker delta, and v_{V_j} is the valency (number of attached edges) at vertex V_j . From here, a graph scattering matrix \hat{S}_Γ can be determined, which performs the mapping between the leads only, i.e.,

$$\mathbf{a}_{\mathcal{L}}^{\text{out}} = \hat{S}_\Gamma(k; L) \mathbf{a}_{\mathcal{L}}^{\text{in}}. \quad (7)$$

Now, \hat{S}_Γ can be constructed from $\hat{\sigma}$ and \hat{P} by

$$\hat{S}_\Gamma(k; L) = \hat{\sigma}_{\mathcal{L}\mathcal{L}} + \hat{\sigma}_{\mathcal{L}\mathcal{B}} \left[\hat{\mathbb{I}} - \hat{P}(k; L) \hat{\sigma}_{\mathcal{B}\mathcal{B}} \right]^{-1} \hat{P}(k; L) \hat{\sigma}_{\mathcal{B}\mathcal{L}}, \quad (8)$$

where $\hat{\mathbb{I}}$ is the identity matrix; see [9] for more details.

Below are the results of solving (8) for each resonant element shown in Fig. 1, i.e.,

$$\hat{S}_{\Gamma_0} = \frac{1}{2} \hat{\mathbb{E}}^{(4 \times 4)} - \hat{\mathbb{I}}^{(4 \times 4)}, \quad (9)$$

$$\hat{S}_{\Gamma_1} = \frac{1}{3} \hat{\mathbb{E}}^{(6 \times 6)} - \hat{\mathbb{I}}^{(6 \times 6)}, \quad (10)$$

$$\hat{S}_{\Gamma_{\text{phase}}}(k; \ell_y) = \frac{1}{2} \begin{pmatrix} -1 & 1 & e^{\frac{ik\ell_y}{2}} & e^{\frac{ik\ell_y}{2}} \\ 1 & -1 & e^{\frac{ik\ell_y}{2}} & e^{\frac{ik\ell_y}{2}} \\ e^{\frac{ik\ell_y}{2}} & e^{\frac{ik\ell_y}{2}} & -e^{ik\ell_y} & e^{ik\ell_y} \\ e^{\frac{ik\ell_y}{2}} & e^{\frac{ik\ell_y}{2}} & e^{ik\ell_y} & -e^{ik\ell_y} \end{pmatrix}, \quad (11)$$

$$\hat{S}_{\Gamma_{\text{res}}}(k; \ell_{\text{res}}) = \frac{2 \cos(k\ell_{\text{res}})}{3 \cos(k\ell_{\text{res}}) + e^{-ik\ell_{\text{res}}}} \hat{\mathbb{E}}^{(4 \times 4)} - \hat{\mathbb{I}}^{(4 \times 4)}, \quad (12)$$

$$\hat{S}_{\Gamma_x}(k; \ell_{x,\text{res}}) = \frac{2 \cos(k\ell_{x,\text{res}})}{\cos(k\ell_{x,\text{res}}) + e^{-ik\ell_{x,\text{res}}}} \hat{\mathbb{E}}^{(2 \times 2)} - \hat{\mathbb{I}}^{(2 \times 2)}, \quad (13)$$

$$\hat{S}_{\Gamma_y}(k; \ell_{y,\text{res}}) = \frac{2 \cos(k\ell_{y,\text{res}})}{\cos(k\ell_{y,\text{res}}) + e^{-ik\ell_{y,\text{res}}}} \hat{\mathbb{E}}^{(2 \times 2)} - \hat{\mathbb{I}}^{(2 \times 2)}. \quad (14)$$

Here, $\hat{\mathbb{E}}^{(n \times n)}$ represents a square matrix of all ones of dimension n . Having defined the scattering matrices associated with each resonant element, one can now construct the full metamaterial.

2.3. Eigenfunction solutions of the periodic graph

From here, the compact portions of the above graphs are treated simply as frequency-dependent point scatterers. Each scatterer is arranged into a square periodic 2D mesh, where the open leads of each resonant element are truncated to form connections of length ℓ between each compact graph. In addition, resonant elements of the type Γ_x and Γ_y , as shown in Fig. 1, can be placed halfway along an edge in the x - and y -direction, respectively (see Fig. 2). This allows for more freedom in constructing interesting wave dispersion curves. The periodic construction means that all wave solutions at the central vertex of any unit cell nm are translationally invariant up to a phase obeying Bloch's theorem [8],

$$\Psi_{nm}(0) = e^{i(\kappa_x n + \kappa_y m)\ell} \Psi(0). \quad (15)$$

Here, κ_x and κ_y represent the quasi-momentum. The symmetry in each connecting edge allows the horizontal and vertical edge scattering due to Γ_x and Γ_y to be evaluated at $z_r = \ell/2$ and $z_u = \ell/2$, respectively, and we obtain

$$\begin{aligned} \begin{pmatrix} a_l^{\text{in}} \\ a_r^{\text{in}} \end{pmatrix} &= \hat{M}_x(k; \ell_{\text{res}}) \begin{pmatrix} a_l^{\text{out}} \\ a_r^{\text{out}} \end{pmatrix}, \\ \begin{pmatrix} a_d^{\text{in}} \\ a_u^{\text{in}} \end{pmatrix} &= \hat{M}_y(k; \ell_{\text{res}}) \begin{pmatrix} a_d^{\text{out}} \\ a_u^{\text{out}} \end{pmatrix}, \end{aligned} \quad (16)$$

where

$$\begin{aligned} \hat{M}_j(k; \ell_{j,\text{res}}) &:= \\ e^{ik\ell} \begin{pmatrix} e^{-i\kappa_j \ell} & 0 \\ 0 & 1 \end{pmatrix} \hat{S}_{\Gamma_j}(k; \ell_{j,\text{res}}) \begin{pmatrix} e^{i\kappa_j \ell} & 0 \\ 0 & 1 \end{pmatrix} \end{aligned} \quad (17)$$

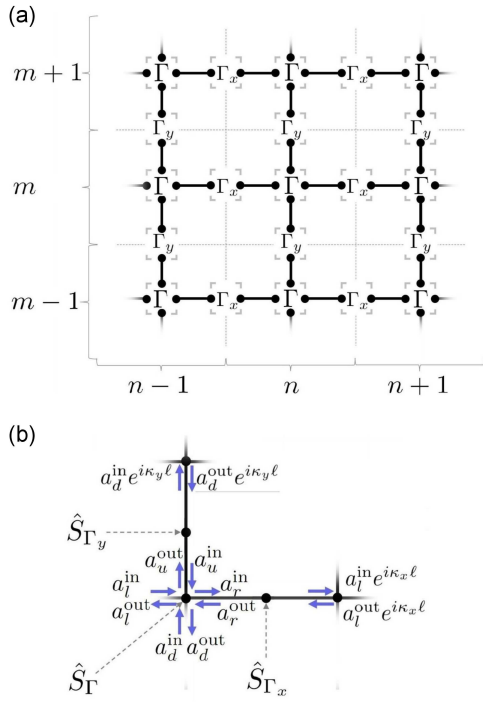


Fig. 2. Panel (a) shows the square periodic arrangement of some arbitrary graph Γ (such as the examples Γ_0 , Γ_{phase} , or Γ_{res}) with mesh indices n , m , spaced by edges of length ℓ . Resonators Γ_x and Γ_y may be placed on both the horizontal and vertical edges. Panel (b) shows the local edge wave amplitudes $a_j^{\text{out/in}}$ represented by blue arrows in the neighbourhood of the central vertex.

with $j = x$ or y and $\ell_{j,res}$ is the resonator length of the edge scattering elements Γ_j . By substitution of (16) into (7), one obtains

$$\left[\hat{\mathbb{I}} - \hat{U}(k, \kappa_x, \kappa_y; L) \right] \mathbf{a}_{\mathcal{L}}^{\text{in}}(k, \kappa_x, \kappa_y; L) = \mathbf{0}, \quad (18)$$

where \hat{U} represents the quantum map and is explicitly given as

$$\hat{U} := \begin{pmatrix} \hat{M}_x & 0 \\ 0 & \hat{M}_y \end{pmatrix} \hat{S}_{\Gamma}. \quad (19)$$

The spectrum of dispersion curves relating k , κ_x , and κ_y are given by solving the secular equation

$$\det \left[\hat{\mathbb{I}} - \hat{U}(k, \kappa_x; \kappa_y, L) \right] = 0. \quad (20)$$

Note that \hat{U} is implicitly a function of the chosen graph metric L . By varying these metric parameters and by changing the topology of the graph Γ , one has great control over the possible wave properties of the metamaterial. We will briefly discuss the examples shown in Fig. 1. A metamaterial constructed purely of elements Γ_0 (i.e., $\ell_{j,res} = 0$ for $j = x$ and y) has in the low-frequency limit an approximately circular dispersion curve modelling free space propagation. As the frequency increases, the underlying square periodic topology becomes “noticeable”, leading to square iso-frequency contours and directional band gaps. The properties of a metamaterial constructed purely of elements Γ_{res} are similar in shape to that of Γ_0 , however, the presence of the edge of length ℓ_{res} opens band gaps, thus forcing high-frequency material properties into the low-frequency domain. The same can be said for the elements Γ_x and Γ_y , where the opening of band gaps is then directional. As for graphs constructed from elements Γ_{phase} , waves travelling from down(up) to up(down) accumulate an additional phase $e^{ik\ell_y}$. This can be thought of as compressing a lattice of period ℓ by $\ell + \ell_y$ to a lattice of period ℓ by ℓ , while maintaining the edge lengths between cells, see Fig. 3. Such a construction breaks the vertex scattering symmetry and allows for negative refraction without relying on resonant characteristics as shown in [9].

2.4. Gaussian beams from graph eigenfunctions

To construct the allowed eigenfunction solutions, we consider a single frequency k and wave number κ_y , leaving in general a choice of two wave numbers κ_x . Naturally, this choice defines the direction of the energy flow. To delineate between waves travelling in opposite horizontal directions, the following notation is used: Eigenfunction solutions with energy flux J_x pointing in the positive x -direction are given an index \rightarrow , and the corresponding eigenvector in (18) is redefined as $\mathbf{a}^{\text{out/in}} := \mathbf{a}^{\text{out/in}}(k, \kappa_x^{\rightarrow}, \kappa_y)$. Eigenfunction solutions with energy flux J_x pointing in the negative x -direction are given an index \leftarrow , and the corresponding eigenvector in (18) is redefined as $\mathbf{b}^{\text{out/in}} := \mathbf{a}^{\text{out/in}}(k, \kappa_x^{\leftarrow}, \kappa_y)$. Explicitly, we write

$$\Psi_{nm} := \begin{cases} \Psi_{nm}^{\rightarrow}(\hat{Z}; k, \kappa_y) = e^{i(\kappa_x^{\rightarrow} n + \kappa_y m)} (e^{ik\hat{Z}} \mathbf{a}^{\text{out}} + e^{-ik\hat{Z}} \mathbf{a}^{\text{in}}), & J_x > 0, \\ \Psi_{nm}^{\leftarrow}(\hat{Z}; k, \kappa_y) = e^{i(\kappa_x^{\leftarrow} n + \kappa_y m)} (e^{ik\hat{Z}} \mathbf{b}^{\text{out}} + e^{-ik\hat{Z}} \mathbf{b}^{\text{in}}), & J_x < 0. \end{cases} \quad (21)$$

For fixed k and κ_y , we thus obtain an eigenfunction solution on the mesh as

$$\Upsilon_{nm}(\hat{Z}; k, \kappa_y) = A(k, \kappa_y) \Psi_{nm}^{\rightarrow}(\hat{Z}; \kappa_y, k) + B(k, \kappa_y) \Psi_{nm}^{\leftarrow}(\hat{Z}; \kappa_y, k), \quad (22)$$

where A and B are wave amplitudes associated with right-hand and left-hand moving waves, respectively. They are both functions of k and κ_y as they will later represent incident and scattered field amplitudes at an interface.

From here, one can construct Gaussian beam solutions Φ_{nm} by integrating over the Brillouin zone (\mathbb{BZ}) of a given metamaterial

$$\Phi_{nm}(\mathbf{z}; k) = \frac{1}{\sqrt{2\pi}} \int_{\mathbb{BZ}} d\kappa_y \alpha(\kappa_y) \Upsilon_{nm}(\hat{Z}, \kappa_y; k), \quad (23)$$

where α is a κ_y -dependent expansion coefficient chosen here to give a Gaussian mode profile, and is defined as

$$\alpha(\kappa_y; \kappa'_y, w) = \gamma \exp \left[-\frac{(\kappa_y - \kappa'_y)^2}{2w^2} \right]. \quad (24)$$

Here, κ'_y determines the direction of the beam relative to the x, y coordinate system, w defines the width of the beam, and γ is a normalisation constant.

3. Wave behaviour at interfaces

3.1. Engineering interface boundary conditions

In previous work [9], the boundary conditions between two different metamaterials modelled by periodic quantum graphs were fixed by satisfying an equivalence condition on the joining edges. In this section, we will demonstrate how to influence the reflection and transmission behaviour at such an interface by introducing an additional boundary layer \mathfrak{B} , as illustrated in Fig. 4a. For this, we consider two infinite half-spaces, each constructed from a square periodic quantum graph with an identical period, as defined in the previous section.

The left half-space represents metamaterial 1 with unit cell $\Gamma^{(1)}$, while the right half-space represents metamaterial 2 with unit cell $\Gamma^{(2)}$. The two metamaterials are coupled via a periodic boundary along the y -direction constructed from either $\Gamma^{(\mathfrak{B})} = \Gamma_{res}$ and $\Gamma^{(\mathfrak{B})} = \Gamma_{y,res}$ or a simple point scatterer with beyond-nearest-neighbour connections, $\Gamma^{(\mathfrak{B})} = \Gamma^{(1)}$, as discussed in [2], see Fig. 4b and c.

The wave properties of the boundary are defined by a scattering matrix $\hat{S}_{\mathfrak{B}}(k, \kappa_y; L)$, which performs the horizontal (H) mapping,

$$\mathbf{a}_H^{\text{out}} = \hat{S}_{\mathfrak{B}}(k, \kappa_y; L) \mathbf{a}_H^{\text{in}}. \quad (25)$$

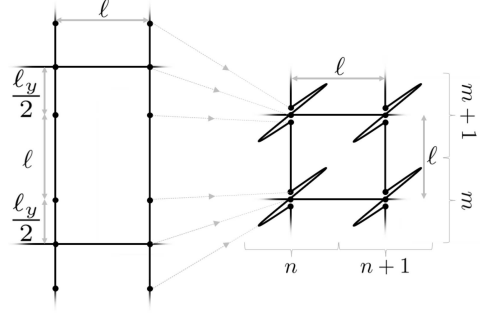


Fig. 3. Illustration of the relationship between the vertex and edge length scale in the case of Γ_{phase} giving rise to non-trivial wave effects.

Here, $\mathbf{a}_H^{\text{out/in}} = (\alpha_l^{\text{out/in}}, \alpha_r^{\text{out/in}})^T$ represents the (to be determined) vector wave amplitudes heading out of or into the boundary vertex on the left (l) or right (r). The boundary scattering matrix is constructed from the underlying vertex scattering matrix as defined in (7), along with the vertical periodicity conditions defined in (16). By decomposing (7) into horizontal (H) and vertical (V) dynamics, one can write

$$\begin{pmatrix} \mathbf{a}_H^{\text{out}} \\ \mathbf{a}_V^{\text{out}} \end{pmatrix} = \begin{pmatrix} \hat{S}_{HH} & \hat{S}_{HV} \\ \hat{S}_{VH} & \hat{S}_{VV} \end{pmatrix} \begin{pmatrix} \mathbf{a}_H^{\text{in}} \\ \mathbf{a}_V^{\text{in}} \end{pmatrix}. \quad (26)$$

One obtains

$$\hat{S}_{\mathfrak{B}} = \hat{S}_{HH} + \hat{S}_{HV} \left[\hat{\mathbb{I}} - \hat{M}_y \hat{S}_{VV} \right]^{-1} \hat{M}_y \hat{S}_{VH}. \quad (27)$$

From this definition, we can determine how the boundary scatters the global wave fields of incident amplitude $A^{(1)}, B^{(2)}$ to give the global scattered field of amplitude $A^{(2)}, B^{(1)}$. To do this, we construct the global boundary scattering matrix $\hat{S}_{\mathfrak{B}}(k, \kappa_y; L)$, which performs the mapping,

$$\begin{pmatrix} B^{(1)} \\ A^{(2)} \end{pmatrix} = \hat{S}_{\mathfrak{B}} \begin{pmatrix} A^{(1)} \\ B^{(2)} \end{pmatrix}. \quad (28)$$

To do this, one substitutes the x component of the eigenfunction solutions (22) on the left and right side of the interface, i.e., at $z_l = z_r = 0$ at the location of the boundary $n = n_{\mathfrak{B}}$ for any m , that is,

$$\begin{aligned} \alpha_l^{\text{out/in}} &= A^{(1)} e^{i(\kappa_x^{(1)} \rightarrow n_{\mathfrak{B}} + \kappa_y m)\ell} a_l^{(1)\text{out/in}} \\ &\quad + B^{(1)} e^{i(\kappa_x^{(1)} \leftarrow n_{\mathfrak{B}} + \kappa_y m)\ell} b_l^{(1)\text{out/in}}, \\ \alpha_r^{\text{out/in}} &= A^{(2)} e^{i(\kappa_x^{(2)} \rightarrow n_{\mathfrak{B}} + \kappa_y m)\ell} a_r^{(2)\text{out/in}} \\ &\quad + B^{(2)} e^{i(\kappa_x^{(2)} \leftarrow n_{\mathfrak{B}} + \kappa_y m)\ell} b_r^{(2)\text{out/in}}, \end{aligned} \quad (29)$$

into (25). After some algebra, we get

$$\begin{aligned} \hat{S}_{\mathfrak{B}} &= \begin{pmatrix} e^{-i\kappa^{(1)} n_{\mathfrak{B}} \ell} & 0 \\ 0 & e^{i\kappa^{(2)} n_{\mathfrak{B}} \ell} \end{pmatrix} \left[\begin{pmatrix} a_l^{(1)\text{out}} & 0 \\ 0 & b_r^{(2)\text{out}} \end{pmatrix} - \hat{S}_{\mathfrak{B}} \begin{pmatrix} a_l^{(1)\text{in}} & 0 \\ 0 & b_r^{(2)\text{in}} \end{pmatrix} \right]^{-1} \\ &\quad \times \left[\hat{S}_{\mathfrak{B}} \begin{pmatrix} b_l^{(1)\text{in}} & 0 \\ 0 & a_r^{(2)\text{in}} \end{pmatrix} - \begin{pmatrix} b_l^{(1)\text{out}} & 0 \\ 0 & a_r^{(2)\text{out}} \end{pmatrix} \right] \begin{pmatrix} e^{-i\kappa^{(1)} n_{\mathfrak{B}} \ell} & 0 \\ 0 & e^{i\kappa^{(2)} n_{\mathfrak{B}} \ell} \end{pmatrix}. \end{aligned} \quad (30)$$

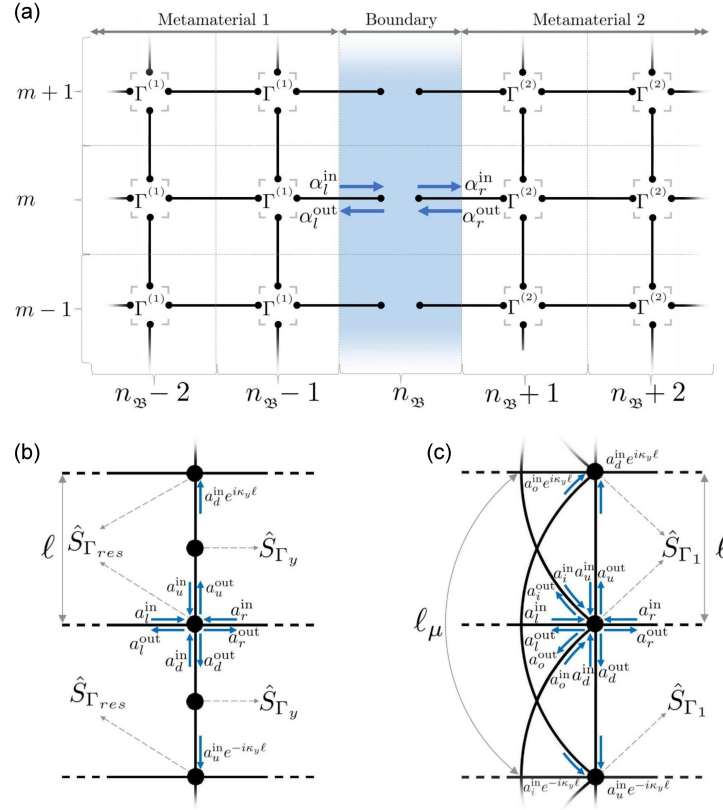


Fig. 4. (a) The boundary region between metamaterials 1 and 2 with amplitudes $\alpha_l^{\text{out/in}}$ and $\alpha_r^{\text{out/in}}$ related by the boundary scattering matrix $\hat{S}_{\mathfrak{B}}$. (b) Boundary constructed of resonators Γ_{res} and Γ_y . (c) Boundary with beyond-nearest-neighbour connections with l_μ , the length of this connection, and μ giving the distance in terms of unit cells; (in the example shown, $\mu = 2$).

3.2. Examples

In the following, we will discuss a few examples leading to interesting reflection/transmission behaviour at interfaces.

3.2.1. Non-reflecting boundaries, beam splitting and steering

In the first example, we will consider how to construct non-reflective interfaces using boundary elements, as shown in Fig. 4b. Here, metamaterial 1 is constructed from elements defined by Γ_0 , while metamaterial 2 is constructed from elements defined by Γ_{res} for $l_{res} = 1.1995\ell$. The corresponding dispersion curves of the two materials are shown in Fig. 5a at $k = 1$. Note that the particular value of l_{res} leads to a square-like dispersion pattern of material 2 with singular behaviour for vanishing κ_x or κ_y . The third plot in Fig. 5a shows the chosen expansion coefficient α giving rise to a beam with width $w = 0.0575$ centred at $\kappa'_y = 1$, which yields an incident Gaussian beam angle of $\theta' = \pi/4$. The chosen boundary is constructed exclusively from Γ_{res} , for $l_{res} = 0\ell$, $l_{res} = 0.9667\ell$, and $l_{res} = \pi\ell/2$ in Fig. 5b–d, respectively.

The transmission $|A^{(2)}|^2$ and reflection coefficients $|B^{(1)}|^2$ of the beam Ψ_{nm} are shown on the RHS of Fig. 5 for panels (b), (c), and (d) as a function of the incident angle θ . This demonstrates that we can obtain both complete transmission and total internal reflection by varying the boundary properties in terms of l_{res} . In particular, total internal reflection happens when $l_{res} = \pi/(2k)$. At this length, the vertex is in resonance, and the boundary conditions reduce to Dirichlet $\hat{S}_{res} = -\hat{\mathbb{I}}$, making the boundary completely reflective.

With this knowledge, we set out to construct a layered metamaterial set-up that will allow us to steer an incoming beam at normal incident around an object. We can do this with minimal reflection at the boundaries using the techniques described above. The example shown in Fig. 6 is made up of four different metamaterials connected by interface layers of the type used in the example shown in Fig. 5. Metamaterials 1 and 4 are identical and are made up of resonant elements Γ_{res} with $l_{res} = 0.725\ell$. The corresponding dispersion curves at $k = 1$ are shown in Fig. 6a. Metamaterial 2 is constructed from both Γ_0 and Γ_y with $l_{y,res} = 0.909175\ell$; note that the material exhibits a corner singularity in its dispersion curve for normal incident giving rise to the beam split-

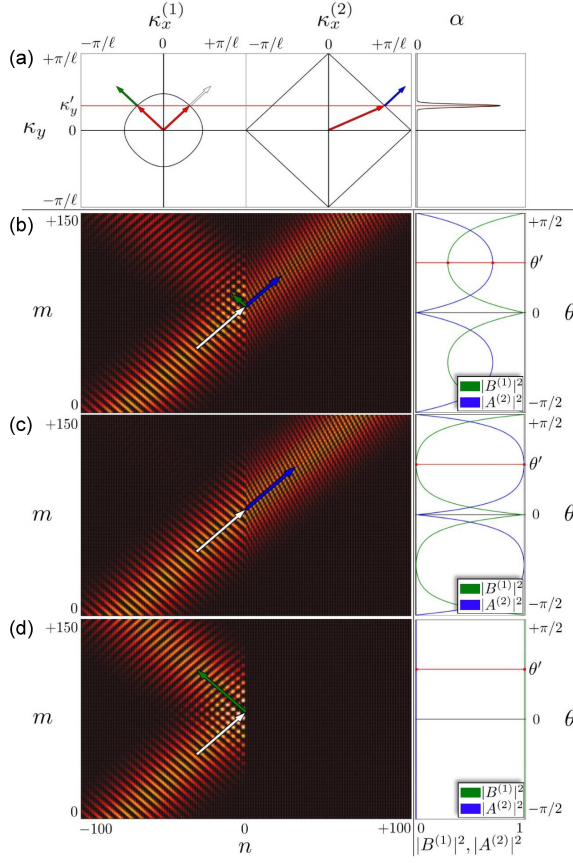


Fig. 5. (a) Isofrequency contours associated with metamaterial 1 and 2 for $k = 1$ together with the Gaussian beam expansion coefficients α . (b)–(d) Reflection behaviour of the beam for different l_{res} chosen at the boundary, see text for details.

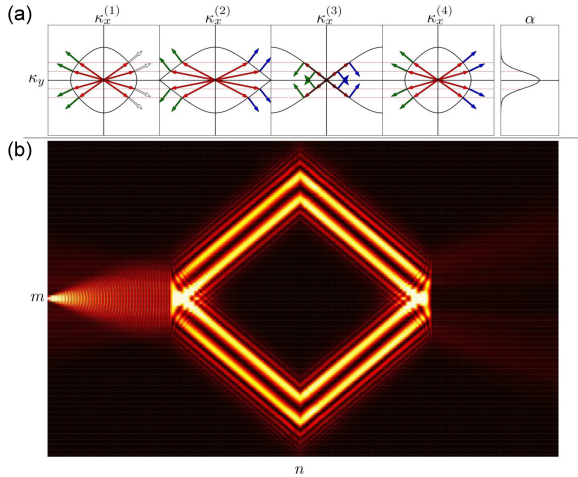


Fig. 6. The plots in (a) show the iso-frequency contours associated with metamaterials 1, 2, 3, and 4, while the 5th plot shows the chosen expansion coefficient α for the incident beam. The plot in (b) displays the resulting norm squared wave amplitude of the incoming and scattered beam $|\Phi_{nm}|^2$. The material interfaces are optimized to give minimal reflection.

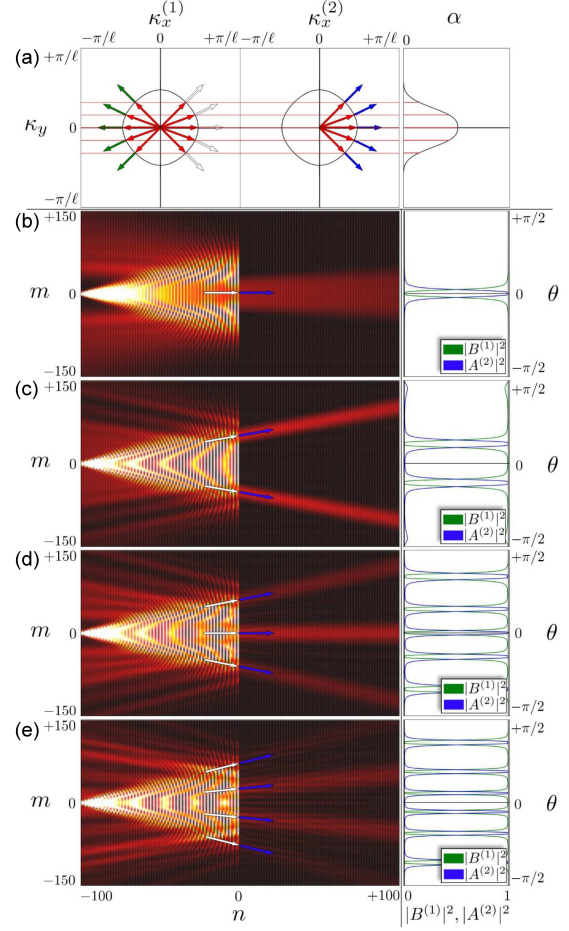


Fig. 7. (a) Dispersion curves of metamaterials 1 and 2 together with the beam shape α for the beam incoming from the LHS. (b)–(e) Wave patterns given by $|\Phi_{nm}|^2$, for different configurations (left) and the reflection/transmission coefficients at the interface as function of the incoming angle θ (right); the parameters are (b) $\mu = 3$, $l_{\mu=3} = 6.32757\ell$; (c) $\mu = 6$, $l_{\mu=6} = 9.3\ell$; (d) $\mu = 10$, $l_{\mu=10} = 12.41818\ell$; (e) $\mu = 12$, $l_{\mu=12} = 15.96\ell$.

ting behaviour observed in Fig. 6b. Metamaterial 3 is constructed from Γ_{phase} and Γ_x for $l_y = 4.64\ell$ and $l_{x,res} = 2.7955\ell$. The metamaterial is designed in such a way as to reverse the beam splitting behaviour yielding negative reflection (see the relevant dispersion curve). We may regard such a device as a primitive cloak in the sense that one can hide or shield an object from normal incidence.

3.2.2. An angle filtering boundary

In the previous example, only nearest-neighbour coupling has been used in the vertical direction of the boundary such as shown in Fig. 4b, that is, a cell m is coupled to cells $m \pm 1$ only. We will now study the properties of an interface boundary made up of the elements shown in Fig. 4c, i.e., we consider $\Gamma^{(3)} = \Gamma_1$, and we connect up the vertices by

using beyond-nearest-neighbour interaction. In the example in Fig. 4c, the next-to-nearest-neighbour coupling is used, that is, in addition to the nearest neighbours, cell m is also coupled to cells $m \pm \mu$ with $\mu = 2$, here. We will later also consider $\mu > 2$.

By introducing the additional coupling, the valency of a boundary vertex increases by two. The vertex conditions are then given by the vertex scattering matrix \hat{S}_{Γ_1} in (10) with Γ_1 shown in Fig. 1b. To obtain $\hat{S}_{\mathbb{B}}$, we must now redefine \hat{M}_y to include

$$\hat{M}_y = \begin{pmatrix} 0 & e^{i(k-\kappa_y)\ell} & 0 & 0 \\ e^{i(k+\kappa_y)\ell} & 0 & 0 & 0 \\ 0 & 0 & 0 & e^{i(k\ell_\mu - \kappa_y\mu\ell)} \\ 0 & 0 & e^{i(k\ell_\mu + \kappa_y\mu\ell)} & 0 \end{pmatrix}. \quad (32)$$

Here, ℓ_μ represents the length of the lead connecting element m to element $m \pm \mu$. Naturally $\ell_\mu \geq \mu\ell$. This is a free parameter that alters the phase accumulation for the wave propagation along the y -direction. In Fig. 7, we show various examples of the wave behaviour at such an interface. In all cases, metamaterials 1 and 2 are identical here and given by simple point scatters Γ_0 , as shown in Fig. 1a. We have chosen a relatively broad beam profile of the incoming beam, covering a wide range of κ_y values and giving the beam a cone-like appearance. A range of μ and corresponding ℓ_μ values are tested.

Surprisingly, the interface acts as an invisible aperture or angle filtering device, letting the incoming wave pass only at certain angles of incident. The number of incoming directions able to pass the interface increases with the connectivity index μ , as demonstrated in Fig. 7b–e; see the figure caption for details regarding the chosen parameters μ and ℓ_μ . The filtering behaviour is brought about by a transmission function being zero for most angles θ apart from narrow-band transmission windows, see the RHS of Fig. 7. Note that these transmission windows exist here although there are no resonant elements present at either vertices or edges and seem to be an interference effect of the competing vertical channels. We report this behaviour here without further analysis, which will be provided in a forthcoming publication.

4. Conclusions

We have demonstrated applications of a quantum graph approach to modelling metamaterials coupled through structured interfaces, thus providing a fast and efficient tool for aiding the design process for layered metamaterial devices. The reflection and transmission coefficients of complex interfaces can be explicitly calculated in our approach, and

the additional coupling. The structure inherits the same Bloch phase as the unit cell has, and the wave amplitudes as such obey the following conditions

$$\begin{aligned} a_u^{\text{in}} &= e^{ik\ell} e^{-i\kappa_y\ell} a_d^{\text{out}} \\ a_d^{\text{in}} &= e^{ik\ell} e^{i\kappa_y\ell} a_u^{\text{out}} \\ a_i^{\text{in}} &= e^{ik\ell_\mu} e^{-i\kappa_y\mu\ell} a_o^{\text{out}} \\ a_o^{\text{in}} &= e^{ik\ell_\mu} e^{i\kappa_y\mu\ell} a_i^{\text{out}} \end{aligned} \quad (31)$$

and \hat{M}_y becomes

the freedom in choosing the vertex scattering matrices and edge lengths provides a large parameter space for constructing desired material properties. We show in particular that interfaces with minimal reflection or transmission can be designed. Beyond-nearest-neighbour coupling along the interface has been incorporated, which can be used as a single-frequency angular filter, allowing for energy transmission only at specific angles and potentially providing a possibility for a tunable aperture or filter. The examples highlight the potential of quantum graph-based metamaterial and interface design. The tuning of edge lengths and the freedom in assigning the vertex scattering matrices are unique to the graph model presented here and enable an open system description that is cumbersome in other conventional mass-spring models, where either the construction of Green's function or a full time-domain simulation is required.

Acknowledgments

The author(s) would like to thank the Isaac Newton Institute for Mathematical Sciences, Cambridge, for support and hospitality during the program Multiple Wave Scattering supported by EPSRC grant no EP/R014604/1. TML and GT would like to acknowledge funding from the Clean Sky 2 Joint Undertaking under the European Union's Horizon 2020 research and innovation programme under grant agreement number 882842 (Silentprop). GJC gratefully acknowledges financial support from the Royal Commission for the Exhibition of 1851 in the form of a Research Fellowship.

References

- [1] R. Kumar, M. Kumar, J. Singh Chohan, S. Kumar, *Mater. Today* **56**, 3016 (2022).

- [2] Y. Chen, M. Kadic, M. Wegener, *Nature Commun.* **12**, 3278 (2021).
- [3] J.A.I. Martínez, M.F. Groß, Y. Chen, T. Frenzel, V. Laude, M. Kadic, M. Wegener, *Sci. Adv.* **7**, eabm2189 (2021).
- [4] D.B. Moore, J.R. Sambles, A.P. Hibbins, T.A. Starkey, G.J. Chaplain, *Phys. Rev. B* **107**, 144110 (2023).
- [5] G.J. Chaplain, I.R. Hooper, A.P. Hibbins, T.A. Starkey, *Phys. Rev. Appl.* **19**, 044061, (2023).
- [6] Y. Chen, J.L.G. Schneider, M.F. Groß, K. Wang, S. Kalt, P. Scott, M. Kadic, M. Wegener, *Adv. Funct. Mater.* **33**, 2302699 (2023).
- [7] A. Kazemi, K.J. Deshmukh, F. Chen, Y. Liu, B. Deng, H. Chien Fu, P. Wang, *Phys. Rev. Lett.* **131**, 176101 (2023).
- [8] L. Brillouin, *Wave Propagation and Group Velocity*, Academic Press, New York 1960.
- [9] T. Lawrie, G. Tanner, D. Chronopoulos, *Sci. Rep.* **12**, 18006 (2022).
- [10] T. Kottos, U. Smilansky, *Ann. Phys.* **274**, 76 (1999).
- [11] S. Gnutzmann, U. Smilansky, *Adv. Phys.* **55**, 527 (2006).
- [12] G. Berkolaiko, P. Kuchment, *Introduction to Quantum Graphs*, Vol. 186, American Mathematical Soc., 2013.
- [13] C. Brewer, S.C. Creagh, G. Tanner, *J. Phys. A Math. Theor.* **51**, 445101 (2018).
- [14] J. Kempe, *Contemp. Phys.* **44**, 307 (2003).
- [15] G.K. Tanner, in: *Non-Linear Dynamics and Fundamental Interactions: Proceedings of the NATO Advanced Research Workshop on Non-Linear Dynamics and Fundamental Interactions*, Tashkent 2004, Springer, 2006, p. 87.
- [16] B. Hein, G. Tanner, *Phys. Rev. Lett.* **103**, 260501 (2009).
- [17] T. Lawrie, S. Gnutzmann, G. Tanner, arXiv:2309.11251, 2023.
- [18] P. Kuchment, *J. Physics A Math. General* **38**, 4887 (2005).
- [19] P. Exner, S. Nakamura, Y. Tadano, *Lett. Math. Phys.* **112**, 83(2022).
- [20] M. Touboul, Ph.D. thesis, Aix-Marseille Université, 2021.